Physics

Magnetic hysteresis in systems presenting perpendicular anisotropy and Dzyaloshinskii-Moriya interaction

Histerese magnética em sistemas que apresentam anisotropia perpendicular e interação de Dzyaloshinskii-Moriya

Heloísa Süffert Acosta [I] [iD], **Bruno Monteiro Figueiró** [II] [iD],
Artur Harres de Oliveira [II] [iD]

[I]Universidade Federal do Rio Grande do Sul, RS, Brazil
[II]Universidade Federal de Santa Maria, Santa Maria, RS, Brazil

ABSTRACT

Micromagnetic calculations were performed to study the impact of interfacial Dzyaloshinskii–Moriya interaction (iDMI) on the magnetization reversal process of thin films presenting perpendicular magnetic anisotropy (PMA). Systems characterized by low, intermediary or high PMA were explored. As the parameter that controls the intensity of iDMI is increased, significant modifications in the magnetization loops may be observed, mainly associated with the emergence of magnetic domains. Analysing the magnetization spatial distribution, it is verified that the formation of Néel type domain walls and magnetic skyrmions are favored by iDMI.

Keywords: Magnetization reversal mechanisms; Interfacial Dzyaloshinskii–Moriya interaction; Magnetic hysteresis; Magnetic skyrmions

RESUMO

Simulações micromagnéticas foram realizadas para estudar o impacto da interação de Dzyaloshinskii–Moriya interfacial (iDMI) nos processos de reversão da magnetização em filmes finos que apresentam anisotropia magnética perpendicular (PMA). Sistemas que apresentam PMA fraca, intermediária e intensa foram explorados. Conforme o parâmetro que caracteriza a intensidade da iDMI aumenta, modificações significativas podem ser observadas nas curvas de histerese magnética, associadas principalmente ao surgimento de domínios magnéticos. Analisando a distribuição espacial da magnetização, verifica-se que a formação de paredes de domínio do tipo Néel e de skyrmions magnéticos é favorecida pela iDMI.

Palavras-chave: Reversão da magnetização; Interação de Dzyaloshinskii–Moriya interfacial; Histerese magnética; Skyrmions magnéticos

1 INTRODUCTION

Magnetic materials with perpendicular magnetic anisotropy (PMA) have been intensively studied in the past few decades, mainly due to their great potential for technological applications. When compared with materials presenting in-plane anisotropy, for example, they are far superior for spin valves sensors used for read-heads of hard disk drives and in magnetoresistive random access memory devices (Tudu and Tiwari (2017)). Since the observation of magnetic skyrmions in thin films presenting PMA (Fert et al. (2013); Heinze et al. (2011); Krause and Wiesendanger (2016); Soumyanarayanan et al. (2017); Woo et al. (2016); Zhang et al. (2015)), the interest in the topic was further intensified.

A magnetic skyrmion may be described as a local whirl of the spin configuration in a magnetic material. They are particle-like spin textures of topological origin, and promise to revolutionize information and communication technologies (Fert et al. (2017); Nagaosa and Tokura (2013); Sampaio et al. (2013); Yu et al. (2017)). The emergence of magnetic skyrmions is associated with multiple mechanisms (Nagaosa and Tokura (2013)). In non-centrosymmetric magnets, the Dzyaloshinskii–Moriya (DMI) interaction (Dzyaloshinskii (1958); Moriya (1960)) induced by the spinorbit coupling in the absence of inversion symmetry in the crystal allows for the formation of a skyrmion lattice structure when an external magnetic field is applied (Mühlbauer et al. (2009); Nagaosa and Tokura (2013); Yu et al. (2011,1)). In ultrathin magnetic/heavy metal bylayers, the breaking of inversion symmetry at the interface and the strong spin-orbit coupling with the neighbouring heavy metal may induce an antisymmetric exchange, known as interfacial DMI (iDMI) (Fert et al. (2017)). A delicate balance between PMA, iDMI, exchange and magnetostatic interactions may lead to the stabilization of magnetic skyrmions at room temperature, even in the absence of an applied magnetic field (Brandão et al. (2019); Chen et al. (2015); Wei et al. (2021); Yu et al. (2018)). From a technological perspective, this is the desired scenario, and several groups are working on the subject. Current research usually focuses on the spatial distribution of magnetization, using experimental techniques like element specific X-ray magnetic circular dichroism photoemission electron microscopy (Boulle et al. (2016)), magnetic force microscopy (Duong et al. (2019); Tejo et al. (2020)) and magneto-optic Kerr effect (Yu et al. (2018)) to probe the magnetic configuration. Even

though the magnetization reversal process is intimately connected to spin textures, studies on the role of iDMI in such process are lacking.

The hysteretic behaviour of magnetization (M) versus applied magnetic field (H) loops is a fingerprint of irreversible magnetization processes. Even though there is an infinite number of different ways to reach a given $M(H)$ state, a curve measured after proper saturation (Harres et al. (2016)), called major loop, may be used to characterize magnetic materials. Such characterization is based on parameters like the coercive field (H_C) and the remnant magnetization (M_R). The shape of $M(H)$ curves is intimately connected with the system's magnetic anisotropy, saturation magnetization and exchange interactions (Coey (2010)).

In the present study, micromagnetic simulations were performed in order to investigate the magnetic behaviour of thin films presenting PMA and iDMI. We focused on how the iDMI affects the magnetization reversal in three systems that exhibit low, intermediate or high PMA (defined by their anisotropy constant). In each case, the evolution of the $M(H)$ major loops as the parameter associated with iDMI is gradually increased is analyzed.

2 METHOD

We performed micromagnetic calculations to study magnetization reversal in polycrystallyne thin films presenting PMA and iDMI. The micromagnetic GPU-based software package Mumax3 (Vansteenkiste et al. (2014)), which solves the Landau-Lifshitz equation,

$$\frac{\partial \mathbf{m}}{\partial t} = \frac{\gamma}{1 + \alpha^2} \left\{ \mathbf{m} \times \mathbf{H}_{\text{eff}} + \alpha \left[\mathbf{m} \times \left(\mathbf{m} \times \mathbf{H}_{\text{eff}} \right) \right] \right\}, \tag{1}$$

was employed. Here, γ is the gyromagnetic ratio, α the dimensionless damping parameter, and $\mathbf{m}$ the normalized magnetization, that varies in time and space. The effective field $\mathbf{H}_{\text{eff}}$ is proportional to the derivative of the energy density ϵ with respect to $\mathbf{m}$,

$$\mathbf{H}_{\text{eff}} = -\frac{1}{\mu_0 M_{\text{s}}} \frac{\partial \epsilon}{\partial \mathbf{m}}, \tag{2}$$

with M_s being the saturation magnetization. The following contributions to ϵ were considered: Zeeman, exchange interaction, interfacial Dzyaloshinskii–Moriya interaction, uniaxial anisotropy, and demagnetizing energy. The effective field term associated with Zeeman energy is simply the external applied field $\mathbf{H}$. Terms associated with each of the remaining energies may be written (Leliaert et al. (2014); Mulkers et al. (2017); Vansteenkiste et al. (2014)), respectively, as follows,

$$\mathbf{H}_{\text{ex}} = \frac{2A_{\text{ex}}}{M_{\text{s}}}\Delta\mathbf{m}\,, \tag{3}$$

$$\mathbf{H}_{\text{DMI}} = \frac{2D}{M_{\text{s}}}\left(\frac{\partial m_z}{\partial x}, \frac{\partial m_z}{\partial y}, -\frac{\partial m_x}{\partial x} - \frac{\partial m_y}{\partial y}\right)\,, \tag{4}$$

$$\mathbf{H}_{\text{anis}} = \frac{2K_{\text{u}}}{M_{\text{s}}}(\mathbf{u}\cdot\mathbf{m})\mathbf{u} + \frac{4K_{u2}}{M_{\text{s}}}(\mathbf{u}\cdot\mathbf{m})^3\mathbf{u}\,, \tag{5}$$

and

$$\mathbf{H}_{\text{demag}} = \hat{\mathbf{K}}_{ij} * \mathbf{M}\,. \tag{6}$$

Here, A_{ex} represents the exchange stiffness, D is the iDMI parameter, K_{u} and K_{u2} are the first and second-order uniaxial anisotropy constants, respectively, and $\mathbf{u}$ an unit vector indicating the anisotropy direction. The quantity $\hat{\mathbf{K}}$ is the demagnetizing kernel. In all calculations, we considered $K_{u2} = 0$, $A_{\text{ex}} = 15$ pJ/m and $M_S = 2.9$ MA/m. These parameters are consistent with those reported for Co/Pd multilayers presenting PMA (Brandão et al. (2019)). The system was simulated as a $512 \times 512 \times 1$ grid of cubic cells. The dimensions of each cell were chosen as $3\,\text{nm} \times 3\,\text{nm} \times 3\,\text{nm}$, each edge being always smaller than the exchange length $l_{\text{ex}} = \sqrt{2A_{\text{ex}}/\mu_0 M_S^2}$. Periodic boundary conditions were considered.

In addition, we have considered the crystalline quality of typical films relevant for applications. It is well known that epitaxially grown systems are not easily compatible with typical spintronic technologies. Therefore, polycrystallyne films grown by sputtering emerge as good candidates for future applications. Aiming at

reproducing the behaviour of such systems, the grid plane was separated in regions through Voronoi tessellation (Leliaert et al. (2014)). Each region plays the role of a grain, being characterized by individual anisotropy parameters. This process is executed using the function `ext_makegrains()`. The grain size is defined by the `grainSize` parameter, that was kept equal to 12 nm for all calculations. The uniaxial anisotropy constant of a grain i is determined according to the following expression,

$$K_u^i = K_u + \eta \times \frac{K_u}{20}, \tag{7}$$

being η a function that returns a normally distributed random number [η is obtained using the Mumax3 command `randNorm()`]. This distribution has mean value 0 and standard deviation 1. Anisotropy axis orientations are also randomly distributed, presenting small deviations from the z axis, that is perpendicular to the film plane. For a given grain i, we define $\mathbf{u}_i$ as a vector

$$\mathbf{u}_i = \left(\frac{\eta}{10}, \frac{\eta}{10}, 1\right), \tag{8}$$

that is subsequently normalized.

To calculate each hysteresis loop, we first set our system in a saturated state, i.e., the magnetization of all cells pointing in the $+\hat{z}$ direction. A 5 T external magnetic field is then applied along the z axis and the minimum energy state is obtained using the built-in function `relax()`. The magnetic field magnitude is reduced by a small value, and a new equilibrium state is obtained using the same function. The process is repeated until a -5 T field is reached. The ascending branch is calculated in an analogous form, starting from a saturated state where all magnetization vectors point in the $-\hat{z}$ direction.

It should also be noted that the `relax()` function attempts to find the system's energy minimum, disabling the precession term in Eq. (1) and turning off excitations like temperature, electrical current and time-dependent magnetic fields. The function advances in time until the total energy cuts into the numerical noise floor, leading the system to a state close to equilibrium. After that, the torque magnitude is monitored instead of energy, and the function runs until the torque cuts into the noise floor as well (Vansteenkiste et al. (2014)).

To study the impact of iDMI on the magnetization reversal process, hysteresis

loops were calculated for different values of D, keeping other parameters fixed. Three scenarios were simulated, considering $K_u = 30$ kJ/m^3, $K_u = 60$ kJ/m^3 and $K_u = 90$ kJ/m^3. For the smaller K_u value, the effective anisotropy constant

$$K_0 = K_u - \frac{1}{2}\mu_0 M_S^2 , \tag{9}$$

is negative, so the effective anisotropy axis is not normal to the system's plane. We shall call this a low PMA case. For $K_u = 60$ kJ/m^3, K_0 assumes a small positive value, and the system presents an intermediary PMA. Finally, when $K_u = 90$ kJ/m^3, $K_0 \gg 0$, characterizing a high PMA configuration. In each case, D was varied between 0.1 mJ/m^2 and 2.0 mJ/m^2. The complete collection of calculated magnetization curves may be found in Figs. 5, 6 and 7 of appendix 4.

3 RESULTS

In Fig. 1, representative results obtained for low PMA and (a) $D = 1.0$ mJ/m^2, (b) $D = 1.1$ mJ/m^2, (c) $D = 1.6$ mJ/m^2 are displayed. The insets show snapshots of the magnetization spatial distribuition for different applied field values. All snapshots correspond to states achieved along the curve's descending branch, that are indicated by solid circles. In these illustrations, the white color represents sample regions where $\mathbf{M}$ is oriented in $+\hat{z}$ direction, and black those oriented in $-\hat{z}$ direction. Other colors represent the magnetization in-plane orientation, also indicated by arrows. The relation between each color and the associated in-plane direction is given in the color map illustrated in the inset of Fig. 1(a).

Magnetization loops similar to that illustrated in Fig. 1(a) were obtained when $D \leq 1.0$ mJ/m^2. Saturation is achieved for $H \approx 0.2$ T, which is very close to the average anisotropy field $H_u = 2K_u/M_S$. The $M(H)$ curve is nearly a straight line between $+0.2$ and -0.2 T, H_C and M_R being approximately zero. In these cases, magnetization rotates toward the system's plane as the field is decreased. This fact may be understood considering that the effective anisotropy K_0 is negative, therefore the system's magnetization presents the tendency to remain in-plane. At same time, the magnetic moment's in-plane orientation changes coherently during the process, indicating that the formation of magnetic domains is not energetically favorable.

Figure 1 – Representative hysteresis loops calculated considering low anisotropy and (a) $D = 1.0$ mJ/m^2, (b) $D = 1.1$ mJ/m^2, (c) $D = 1.6$ mJ/m^2, along with snapshots of the magnetization spatial distribuition for different values of the external applied field
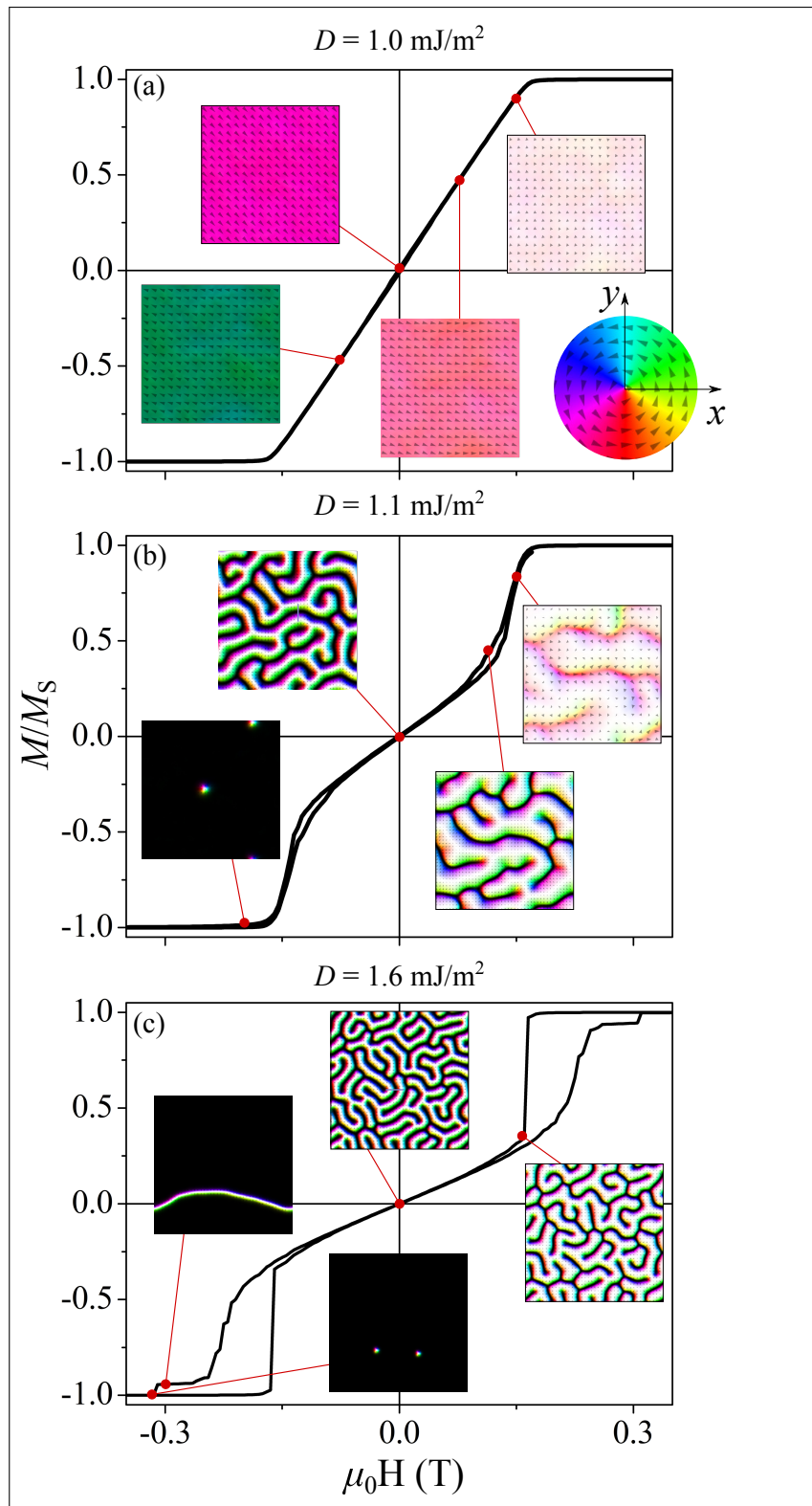
Snapshots illustrate the whole system area
Source: the authors (2024)

Figure 2 – Representative hysteresis loops calculated considering intermediary anisotropy and (a) $D = 0.4$ mJ/m^2, (b) $D = 0.6$ mJ/m^2, (c) $D = 1.4$ mJ/m^2, along with snapshots of the magnetization spatial distribuition for different applied field values
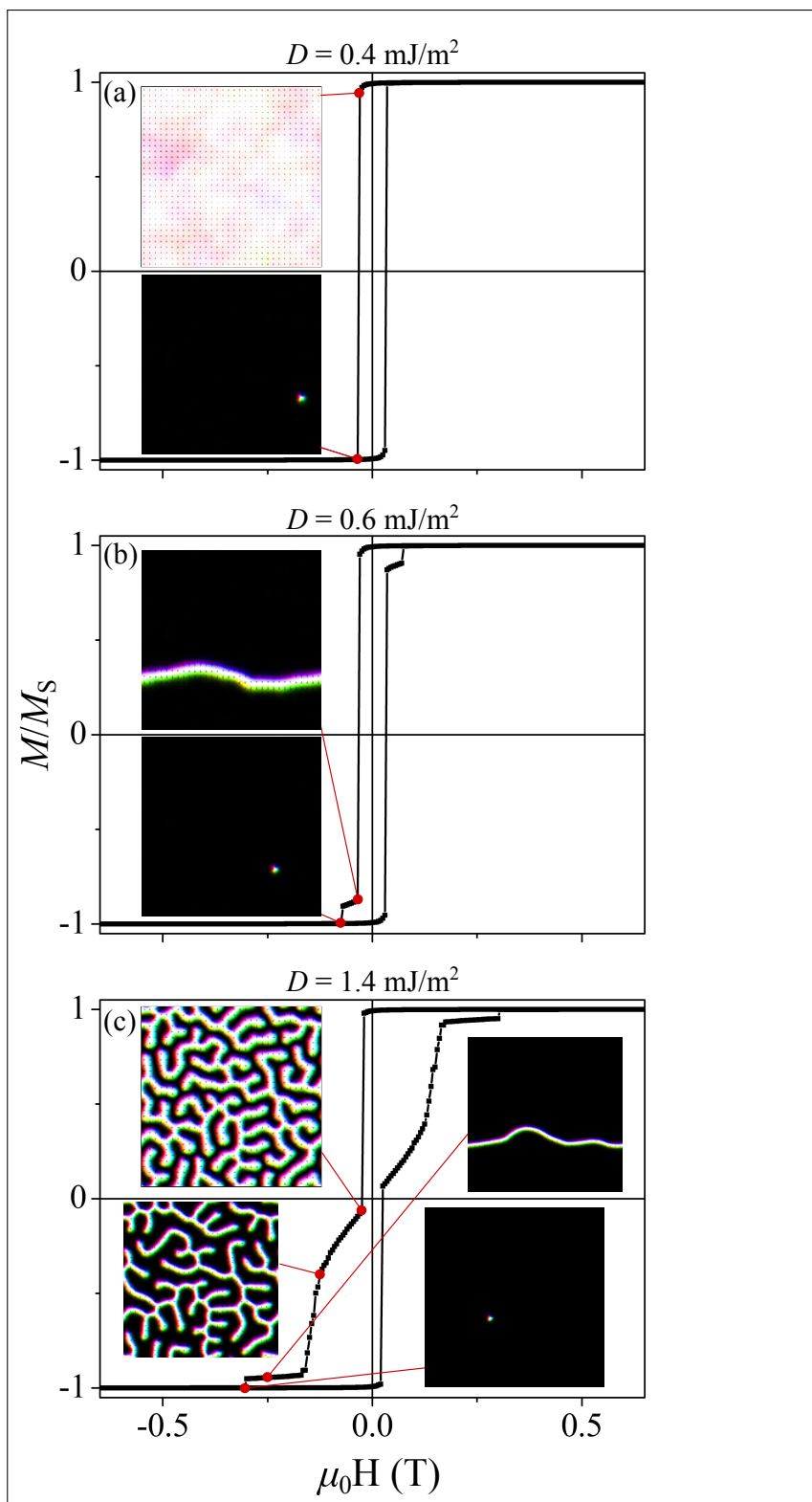
Note: Snapshots illustrates the whole system area
Source: the authors (2024)

Interestingly, by increasing D to 1.1 mJ/m^2, we see that the hysteresis shape is modified, as shown in Fig. 1(b). Starting from the saturated state, the magnetic configuration gradually evolves into a maze-like domain structure. Reversed domains grow, and when H becomes zero, out-of-plane magnetization is also zero. As saturation is approached in the opposite direction, small circular domains may be observed. A closer look reveals that these domains are Néel-type skyrmions [see Fig. 4(c)]. A similar behavior is obtained for $D = 1.2$ and 1.3 mJ/m^2. The necessity to apply an external field to stabilize skyrmions has been previously demonstrated by an analytical model that incorporates all the energies into play (Bernand-Mantel et al. (2018)).

Although M_R is zero for curves obtained for both $D = 1.0$ and 1.1 mJ/m^2, their magnetization spatial distribution at $H = 0$ is completely distinct. In the first case, magnetic moment's are parallel to sample's plane, while in the second the majority of spins are oriented along the z axis, either in $+\hat{z}$ or $-\hat{z}$ directions. This behaviour is related to the fact that iDMI facilitates the formation of Néel domain walls, what will be further discussed in Section 4.

A magnetization loop traced for $D = 1.6$ mJ/m^2 is illustrated in Fig. 1(c). In this case, the evolution from a saturated state into a maze-like domain configuration is abrupt. As the external field decreases, reversed domains grow and a $M_R = 0$ state is reached. Increasing the field in the opposite direction leads to a stripe-domain configuration that corresponds to a plateau in the magnetization curve. Finally, skyrmions are stabilized close to saturation.

Representative results obtained for intermediary PMA and (a) $D = 0.4$ mJ/m^2, (b) $D = 0.6$ mJ/m^2, (c) $D = 1.4$ mJ/m^2 are shown in Fig. 2. For D values between 0.1 and 0.3 mJ/m^2, the magnetization loops are square shaped, indicating a well defined out-of-plane easy axis. An abrupt magnetization reversal is observed; the system evolves from a saturated state in one direction to a saturated state in an opposite direction whitin an infinitesimal change of the external field. The loop obtained for $D = 0.4$ mJ/m^2, illustrated in Fig. 2(a), is nearly indistinguishable from those traced for $D \leq 0.3$ mJ/m^2, but a state where a skyrmion is stabilized is reached after the magnetization jump. Increasing D to 0.5 mJ/m^2, a distinguished feature appears in the loop as a plateau is achieved after the magnetization jump. This plateau, that persists

within a small external field range, corresponds to a stripe domain. As the field increases, the stripe eventually vanishes, and after another abrupt variation of $M(H)$, a Néel-type skyrmion appears and persists for a narrow field range. The magnetization curve shown in Fig. 2(b), that was traced for $D = 0.6$ mJ/m², has the same characteristics.

The appearance of magnetization loops gradually changes as D varies from 0.7 mJ/m² up to 2.0 mJ/m², acquiring a shape that resembles an hourglass. A representative curve obtained for $D = 1.4$ mJ/m² is displayed in Fig. 2(c). We observe now that after the abrupt variation of M, a maze-like domain configuration is achieved. Reversed domains gradually grow as the external field magnitude is increased, and evolve into a stripe domain, similar to that obtained for $D = 0.6$ mJ/m². As in the previous case, a skyrmion is stabilized for fields close to saturation.

Figure 3 brings representative magnetization curves calculated considering high PMA and (a) $D = 1.1$ mJ/m², (b) $D = 1.7$ mJ/m², (c) $D = 2.0$ mJ/m². For D values ranging from 0.1 up to 0.9 mJ/m², we observe square-shaped hysteresis loops similar to those obtained for $K_u = 60$ kJ/m² and low values of D. Since the anisotropy constant was increased compared to the previously presented cases, the anisotropy energy term dominates the magnetic behaviour, and the iDMI contribution begins to become important only for $D \geq 1.0$ mJ/m². For $D = 1.0$ and 1.1 mJ/m², calculated curves still present the same square shape, as illustrated in Fig. 3 (a), but after the abrupt variation of $M(H)$, a magnetic state with skyrmions is obtained. Further increasing the iDMI parameter will lead to the appearence of a plateau in the magnetization curve, as shown in Fig. 3(b) for $D = 1.7$ mJ/m². In such state, we may observe interconnected stripe domains that slowly fade as the external field magnitude is increased until another abrupt magnetization variation occurs. Differently from the case of intermediary PMA, no skyrmions are stabilized after this second jump. Finally, for $D = 1.9$ and 2.0 mJ/m², a maze-like domain state is reached after the magnetization jump. This state evolves into a stripe domain configuration as the external field is increased, as shown in figure Fig. 3 (c). Further increasing H, we see an abrupt variation of M and a plateau appears. As was the case for $K_u = 30$ and 60 kJ/m², this feature is associated with a state presenting a single stripe domain.

Figure 3 – Representative hysteresis loops calculated considering high anisotropy and (a) $D = 1.1$ mJ/m^2, (b) $D = 1.7$ mJ/m^2, (c) $D = 2.0$ mJ/m^2, along with snapshots of the magnetization spatial distribuition for different values of the external applied fiel
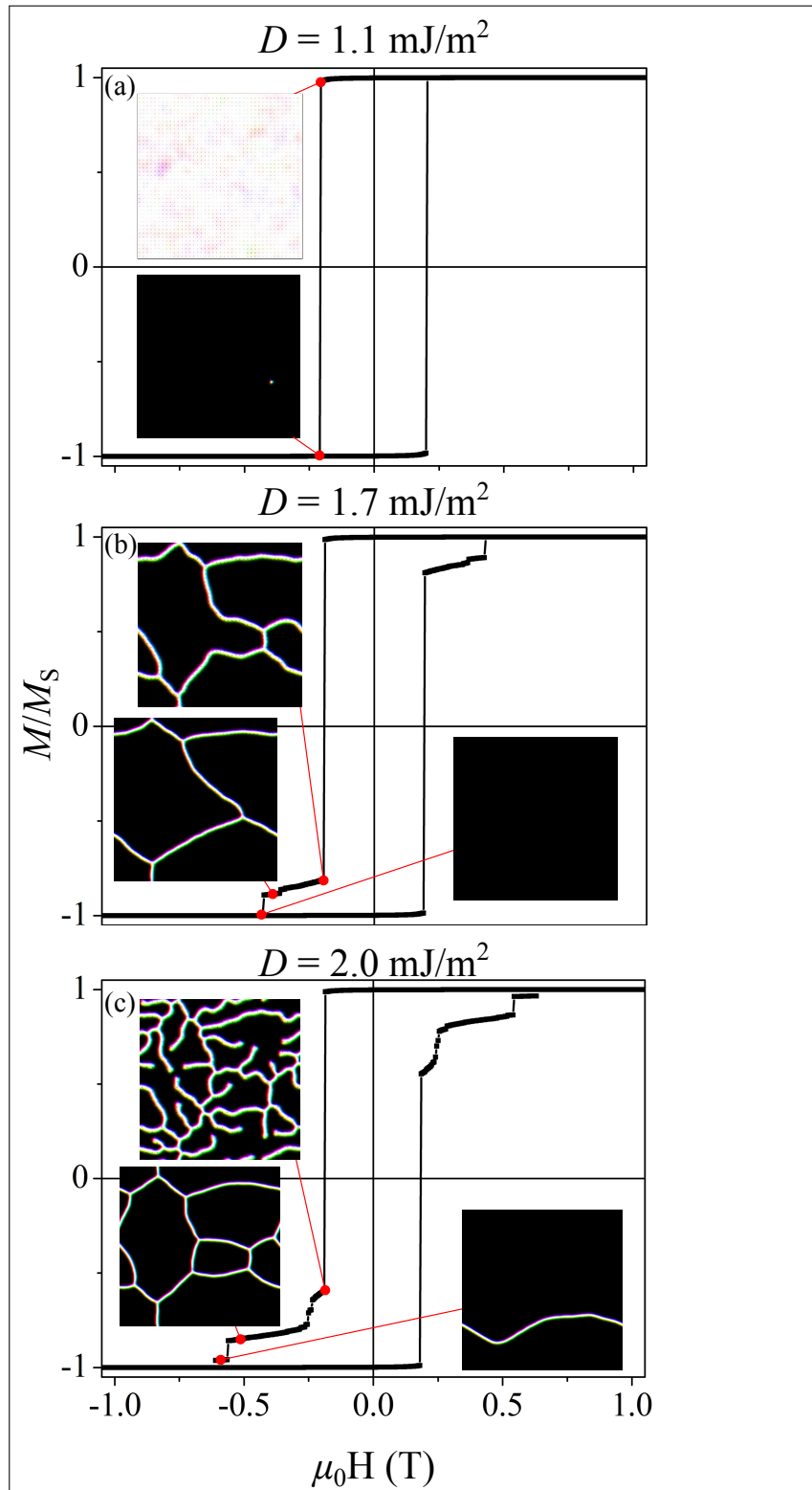

Note: Snapshots illustrates the whole system area
Source: the authors (2024)

4 DISCUSSION

The shape of magnetization curves and it's associated domain structure results from a competition between various energy terms. The PMA tends to align the magnetization in a direction normal to the film plane, while exchange interaction favors parallel alignment of neighbouring spins. A saturated state along the z-axis, however, sets up magnetic poles at the top and bottom surfaces of the film, increasing the magnetostatic energy. The creation of magnetic domains may decrease the magnetostatic energy, but add domain wall energy (Málek and Kamberský (1958)). Finally, the iDMI induces a relative tilt between neighbouring spins. It may facilitate the formation of domains by lowering the domain wall energy (Heide et al. (2008); Woo et al. (2016)), and stabilize magnetic skyrmions (Fert et al. (2017)). This is what is observed as iDMI is increased in our calculations. For low PMA and $D \leq 1.0$ mJ/m^2, even though the average uniaxial anisotropy axis is oriented out-of-plane, the anisotropy constant is too small and the magnetostatic energy term dominates, pushing the magnetization to the plane for a low value of H. The exchange interaction guarantees that magnetization evolves coherently, without breaking up into domains, resulting in curves like the one shown in Fig. 1(a). For both intermediary and high PMA, exchange and anisotropy terms dominate when D is small, leading to square-shaped hysteresis curves illustrated in Figs. 2(a) and 3(a). The system abruptly transits from a saturated state in one out-of-plane direction to a saturated state in the opposite direction, as the formation of magnetic domains is not energetically favourable.

When D is increased to 1.1 mJ/m^2 for low PMA, the iDMI becomes relevant, lowering the domain wall energy and allowing a labyrinthine structure to take place. The magnetization curve becomes skewed, and hysteresis is present for intermediary fields, as shown in Fig. 1(b). Calculated loops resemble experimental curves obtained for Pt/Co/Fe/Ir multilayers presenting iDMI and thicknesses compatible with that considered in the present paper (Ang et al. (2021)), or thicker (Duong et al. (2019)). The simulated evolution of magnetization spatial distribuion is also coherent with data presented in Fig. 1(c) of reference (Ang et al. (2021)). Similar magnetization curves may also be observed for Co/Pt (Hellwig et al. (2007)) and Co/Pd (Brandão et al. (2019)) samples, where the iDMI should be absent, or small (Hrabec et al. (2014)), due to the symmetrical interfaces. In such cases, though, skewed curves occur for thicker films.

Figure 4 – Representative regions of the magnetization spatial distribution obtained for $K_u = 30$ kJ/m³, $H = 0$, (a) $D = 1.1$ mJ/m² and (b) 1.6 mJ/m². (c) A Néel type skyrmion observed for $K_u = 60$ kJ/m³ and $D = 0.4$ mJ/m²
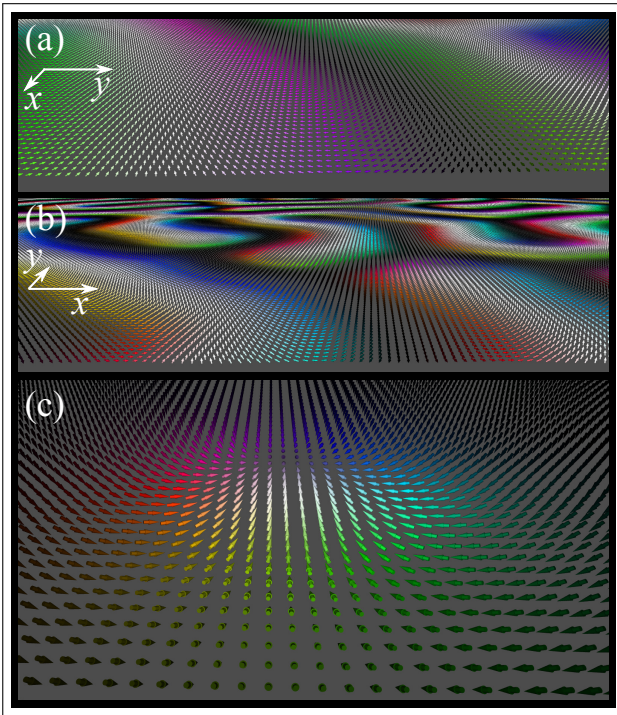
Source: the authors (2024)

Considering $D \geq 1.4$ mJ/m², the skewed shape of $M(H)$ persists, hysteresis is enhanced and a plateau associated with a stripe domain configuration may be observed, as depicted in Fig. 1(c). Most of these features are present in experimental curves obtained for thin films presenting PMA (Davies et al. (2004); Hellwig et al. (2007)). The hourglass-like shape obtained for intermediary PMA and high iDMI may also be observed in real systems (Brandão et al. (2019); Skorokhodov et al. (2021); Yim et al. (2004)).

Most of the characteristics aquired by the magnetization loops as D is increased may also be observed in systems where iDMI is absent. Therefore, we were not able to identify any signature of interfacial Dzyaloshinskii–Moriya interaction in these curves. An exception may be the plateau associated with a single stripe-domain state, observed in Figs. 1(c), 2(b) and (c), and 3(c). We found no report of experimental magnetization loops presenting that feature. Our hypothesis is that the simulated system dimensions are too small, and even though such domains occurs in real samples, they might be too scarce to have an impact in the measured $M(H)$ curve. In such case, the plateau would

be less pronounced or even invisible. See, for example, figure 2(g) in reference (Davies et al. (2004)).

Finally, let us briefly discuss the nature of the magnetic structures obtained in our caculations. Figures[1] 4(a) and 4(b) depict representative regions of the magnetization spatial distributions illustrated in Figs. 1(b) and 1(c) for $H = 0$. As may be seen, iDMI favors Néel type domain walls (DW), *i.e.*, the magnetization rotates in a cycloidal mode, with the DW normal contained in the magnetization rotation plane. The same behaviour is observed for high PMA. This result is in accordance with the model introduced by Heide, Bihlmayer and Blügel (Heide et al. (2008)), and expanded by Thiaville *et al.* (Thiaville et al. (2012)). They have shown that Néel DW are more likely to form in thin films presenting iDMI. Figure 4(c) shows that the circular structures observed in the inset of 2(a) is, indeed, a Néel type skyrmion, where spins rotate in the radial planes from the core to the periphery. Skyrmions observed for other parameters are of the same type.

In summary, we studied the impact of iDMI on magnetization reversal processes in thin films presenting PMA via micromagnetic calculations. Three distinct scenarios, characterized by low, intermediary or high perpendicual anisotropy were explored. We observed in all of them that the energy landscape shifts as D is increased, allowing the stabilization of skyrmions, stripe and/or maze-like domains presenting Néel DW. The magnetization loops shape is significantly modified, and distinct features appears for the different K_u values considered.

ACKNOWLEDGEMENTS

---

[1]Figures obtained through the web application Mumax-View, available at https://mumax.ugent.be/mumax-view/

REFERENCES

Ang, C. C. I., Gan, W., Wong, G. D. H., & Lew, W. S. (2021). Temperature-modulated magnetic skyrmion phases and transformations analysis from first-order reversal curve study. *Physical Review B*, *103*, 144409. Recovered from: https://doi.org/10.1103/PhysRevB.103.144409.

Bernand-Mantel, A., Camosi, L., Wartelle, A., Rougemaille, N., Darques, M., & Ranno, L. (2018). The skyrmion-bubble transition in a ferromagnetic thin film. *SciPost Phys.*, *4*, 027. Recovered from: https://doi.org/10.21468/SciPostPhys.4.5.027:027.

Boulle, O., Vogel, J., Yang, H., Pizzini, S., Chaves, D. S., Locatelli, A., Menteş, T. O., & Gaudin, G. (2016). Room-temperature chiral magnetic skyrmions in ultrathin magnetic nanostructures. *Nature Nanotechnology*, *11*, 449-454. Recovered from: https://doi.org/10.1038/nnano.2015.315.

Brandão, J., Dugato, D. A., Seeger, R. L., Denardin, J. C., Mori, T. J. A., & Cezar, J. C. (2019). Observation of magnetic skyrmions in unpatterned symmetric multilayers at room temperature and zero magnetic field. *Scientific Reports*, *9*, 4144. Recovered from: https://doi.org/10.1038/s41598-019-40705-4.

Chen, G., Mascaraque, A., N'Diaye, A. T., & Schmid, A. K. (2015). Room temperature skyrmion ground state stabilized through interlayer exchange coupling. *Applied Physics Letters*, *106*, 242404. Recovered from: https://doi.org/10.1063/1.4922726.

Coey, J. M. D. (2010). *Magnetism and Magnetic Materials*. Cambridge University Press.

Davies, J. E., Hellwig, O., Fullerton, E. E., Denbeaux, G., Kortright, J. B., & Liu, K. (2004). Magnetization reversal of Co/Pt multilayers: Microscopic origin of high-field magnetic irreversibility. *Physical Review B*, *70*, 224434. Recovered from: https://doi.org/10.1103/PhysRevB.70.224434.

Duong, N. K., Raju, M., Petrović, A. P., Tomasello, R., Finocchio, G., & Panagopoulos, C. (2019). Stabilizing zero-field skyrmions in Ir/Fe/Co/Pt thin film multilayers by magnetic history control. *Applied Physics Letters*, *114*, 072401. Recovered from: https://doi.org/10.1063/1.5080713.

Dzyaloshinskii, I. (1958). A thermodynamic theory of "weak" ferromagnetism of antiferromagnetics. *Journal of Physics and Chemistry of Solids*, *4*241. Recovered from: https://doi.org/10.1016/0022-3697(58)90076-3.

Fert, A., Cros, V., & Sampaio, J. (2013). Skyrmions on the track. *Nature Nanotechnology*, *8*, 152-156. Recovered from: https://doi.org/10.1038/nnano.2013.29.

Fert, A., Reyren, N., & Cros, V. (2017). Topological properties and dynamics of magnetic skyrmions. *Nature Reviews Materials*, *2*, 17031. Recovered from: https://doi.org/10.1038/natrevmats.2017.31.

Harres, A., Mikhov, M., Skumryev, V., de Andrade, A., Schmidt, J., & Geshev, J. (2016). Criteria for saturated magnetization loop. *Journal of Magnetism and Magnetic Materials*, *402*, 76-82. Recovered from: https://doi.org/10.1016/j.jmmm.2015.11.046.

Heide, M., Bihlmayer, G., & Blügel, S. (2008). Dzyaloshinskii-moriya interaction accounting for the orientation of magnetic domains in ultrathin films: Fe/W(110). *Physical Review B*, *78*, 140403(R). Recovered from: https://doi.org/10.1103/PhysRevB.78.140403.

Heinze, S., von Bergmann, K., Menzel, M., Brede, J., Kubetzka, A., Wiesendanger, R., Bihlmayer, G., & Blügel, S. (2011). Spontaneous atomic-scale magnetic skyrmion lattice in two dimensions. *Nature Physics*, *7*, 713–718. Recovered from: https://doi.org/10.1038/nphys2045.

Hellwig, O., Berger, A., Kortright, J. B., & Fullerton, E. E. (2007). Domain structure and magnetization reversal of antiferromagnetically coupled perpendicular anisotropy films. *Journal of Magnetism and Magnetic Materials*, *319*(1), 13-55. Recovered from: https://doi.org/10.1016/j.jmmm.2007.04.035.

Hrabec, A., Porter, N. A., Wells, A., Benitez, M. J., Burnell, G., S. McVitie, D. M., Moore, T. A., & Marrows, C. H. (2014). Measuring and tailoring the dzyaloshinskii-moriya interaction in perpendicularly magnetized thin films. *Physical Review B*, *90*, 020402(R). Recovered from: https://doi.org/10.1103/PhysRevB.90.020402.

Krause, S. & Wiesendanger, R. (2016). Skyrmionics gets hot. *Nature Materials*, *15*, 493-494. Recovered from: https://doi.org/10.1038/nmat4615.

Leliaert, J., de Wiele, B. V., Vansteenkiste, A., Laurson, L., Durin, G., Dupré, L., & Waeyenberge, B. V. (2014). Current-driven domain wall mobility in polycrystalline permalloy nanowires: A numerical study. *Journal of Applied Physics*, *115*, 233903. Recovered from: https://doi.org/10.1063/1.4883297.

Moriya, T. (1960). Anisotropic superexchange interaction and weak ferromagnetism. *Physical Review*, *120*, 91. Recovered from: https://doi.org/10.1103/PhysRev.120.91.

Mulkers, J., Waeyenberge, B. V., & Milošević, M. V. (2017). Effects of spatially engineered dzyaloshinskii-moriya interaction in ferromagnetic films. *Physical Review B*, *95*, 144401. Recovered from: https://doi.org/10.1103/PhysRevB.95.144401.

Málek, Z. & Kamberský, V. (1958). On the theory of the domain structure of thin films of magnetically uni-axial materials. *Cechoslovackij fiziceskij zurnal*, *8*, 416-421. Recovered from: https://doi.org/10.1007/BF01612066.

Mühlbauer, S., Binz, B., Jonietz, F., Pfleiderer, C., Rosch, A., Neubauer, A., Georgii, R., & Böni, P. (2009). Skyrmion lattice in a chiral magnet. *Science*, *323*, 915-919. Recovered from: https://doi.org/10.1126/science.1166767.

Nagaosa, N. & Tokura, Y. (2013). Topological properties and dynamics of magnetic skyrmions. *Nature Nanotechnology*, *8*, 899-911. Recovered from: https://doi.org/10.1038/NNANO.2013.243.

Sampaio, J., Cros, V., Rohart, S., Thiaville, A., & Fert, A. (2013). Nucleation, stability and current-induced motion of isolated magnetic skyrmions in nanostructures. *Nature Nanotechnology*, *8*, 839-844. Recovered from: https://doi.org/10.1038/nnano.2013.210.

Skorokhodov, E., Sapozhnikov, M., Ermolaeva, O., Gusev, N., Fraerman, A., & Mironov, V. (2021). Magnetic resonance force spectroscopy of multilayer films Co/Pt with perpendicular magnetic anisotropy. *Journal of Magnetism and Magnetic Materials*, *518*, 167396. Recovered from: https://doi.org/10.1016/j.jmmm.2020.167396.

Soumyanarayanan, A., Raju, M., Oyarce, A. L. G., Tan, A. K. C., Im, M.-Y., Petrović, A. P., Ho, P., Khoo, K. H., Tran, M., Gan, C. K., Ernult, F., & Panagopoulos, C. (2017). Tunable room-temperature magnetic skyrmions in ir/fe/co/pt multilayers. *Nature Materials*, *16*, 898-904. Recovered from: https://doi.org/10.1038/nmat4934.

Tejo, F., Toneto, D., Oyarzún, S., Hermosilla, J., Danna, C. S., Palma, J. L., da Silva, R. B., Dorneles, L. S., & Denardin, J. C. (2020). Stabilization of magnetic skyrmions on arrays of self-assembled hexagonal nanodomes for magnetic recording applications. *ACS Applied Materials & Interfaces*, *12*(47), 53454-53461. Recovered from: https://doi.org/10.1021/acsami.0c14350.

Thiaville, A., Rohart, S., Émilie Jué, Cros, V., & Fert, A. (2012). Dynamics of dzyaloshinskii domain walls in ultrathin magnetic films. *Journal of Magnetism and Magnetic Materials*, *100*(5), 57002. Recovered from: https://doi.org/10.1209/0295-5075/100/57002.

Tudu, B. & Tiwari, A. (2017). Recent developments in perpendicular magnetic anisotropy thin films for data storage applications. *Vacuum*, 146:329–341.

Vansteenkiste, A., Leliaert, J., Dvornik, M., Helsen, M., Garcia-Sanchez, F., & Waeyenberge, B. V. (2014). The design and verification of mumax3. *AIP Advances*, *4*, 107133. Recovered from: https://doi.org/10.1063/1.4899186.

Wei, Y., Liu, C., Zeng, Z., Wang, X., Wang, J., & Liu, Q. (2021). Room-temperature zero field and high-density skyrmions in Pd/Co/Pd multilayer films. *Journal of Magnetism and Magnetic Materials*, *521*, 167507. doi: https://doi.org/10.1016/j.jmmm.2020.167507.

Woo, S., Litzius, K., Krüger, B., Im, M.-Y., Caretta, L., Richter, K., Mann, M., Krone, A., Reeve, R. M., Weigand, M., Agrawal, P., Lemesh, I., Mawass, M.-A., Fischer, P., Kläui, M., & Beach, G. S. D. (2016). Observation of room-temperature magnetic skyrmions and their current-driven dynamics in ultrathin metallic ferromagnets. *Nature Materials*, *15*, 501-506. Recovered from: https://doi.org/10.1038/nmat4593.

Yim, H. I., Park, J. S., Hwang, J. Y., Lee, S. B., & Kim, T. W. (2004). Perpendicular magnetic anisotropy of CoSiB/Pt multilayers. *Journal of the Korean Physical Society*, *70*, 224434. Recovered from: https://doi.org/10.3938/jkps.57.1672.

Yu, G., Jenkins, A., Ma, X., Razavi, S. A., He, C., Yin, G., Shao, Q., & ... Wang, K. L. (2018). Room-temperature skyrmions in an antiferromagnet-based heterostructure. *Nano Letters*, *18*, 980-986. Recovered from: https://doi.org/10.1021/acs.nanolett.7b04400.

Yu, G., Upadhyaya, P., Shao, Q., Wu, H., Yin, G., Li, X., He, C., & ... Wang, K. L. (2017). Room-temperature skyrmion shift device for memory application. *Nano Letters*, *17*, 261-268. Recovered from: https://doi.org/10.1021/acs.nanolett.6b04010.

Yu, X. Z., Kanazawa, N., Onose, Y., Kimoto, K., Zhang, W. Z., Ishiwata, S., Matsui, Y., & Tokura, Y. (2011). Near room-temperature formation of a skyrmion crystal in thin-films of the helimagnet fege. *Nature Materials*, *10*, 106-109. Recovered from: https://doi.org/10.1038/nmat2916.

Yu, X. Z., Onose, Y., Kanazawa, N., Park, J. H., Han, J. H., Matsui, Y., Nagaosa, N., & Tokura, Y. (2010). Real-space observation of a two-dimensional skyrmion crystal. *Nature*, 465:901–904.

Zhang, X., Zhao, G. P., Fangohr, H., Liu, J. P., Xia, W. X., Xia, J., & Morvan, F. J. (2015). Skyrmion-skyrmion and skyrmion-edge repulsions in skyrmion-based racetrack memory. *Scientific Reports*, *5*, 7643. Recovered from: https://doi.org/10.1038/srep07643.

Author contributions

1 – Heloísa Suffert Acosta
Physicist
https://orcid.org/0000-0002-3848-1183 • fisica.heloisa@gmail.com
Contribution: Methodology; Writing – Review & Editing

2 – Bruno Monteiro Figueiró
Physicist
https://orcid.org/0000-0002-7057-5585 • brunoomf1@gmail.com
Contribution: Literature Review, Data Analysis, Writing – Review & Editing

3 – Artur Harres de Oliveira (Corresponding Author)
Physicist, Professor
https://orcid.org/0000-0002-1439-7702 • artur.harres@ufsm.br
Contribution: Conceptualization, Data Analysis, Writing – Original Draft Preparation

How to cite this article

Acosta, H. S., Figueiró, B. M., Oliveira, A. H. de (2024). Magnetic hysteresis in systems presenting perpendicular anisotropy and Dzyaloshinskii-Moriya interaction. *Ciência e Natura*, Santa Maria, v.46, e84494. https://doi.org/10.5902/2179460X84494

Appendix - Hysteresis loops

Figures 5, 6 and 7 display the full collection of magnetization loops calculated, respectively, for the low, intermediary and high PMA scenarios.

Figure 5 – Hysteresis loops obtained for low anisotropy
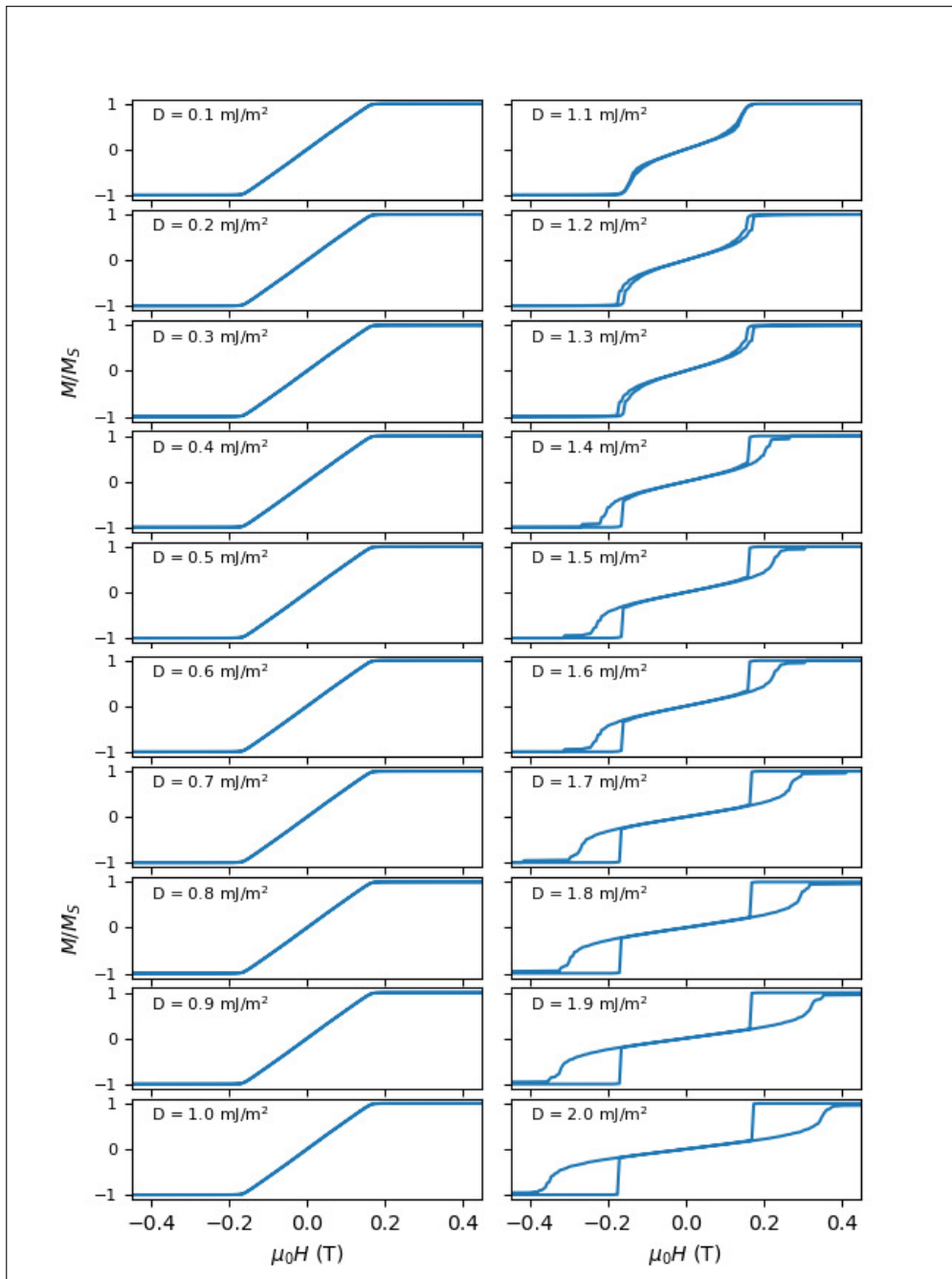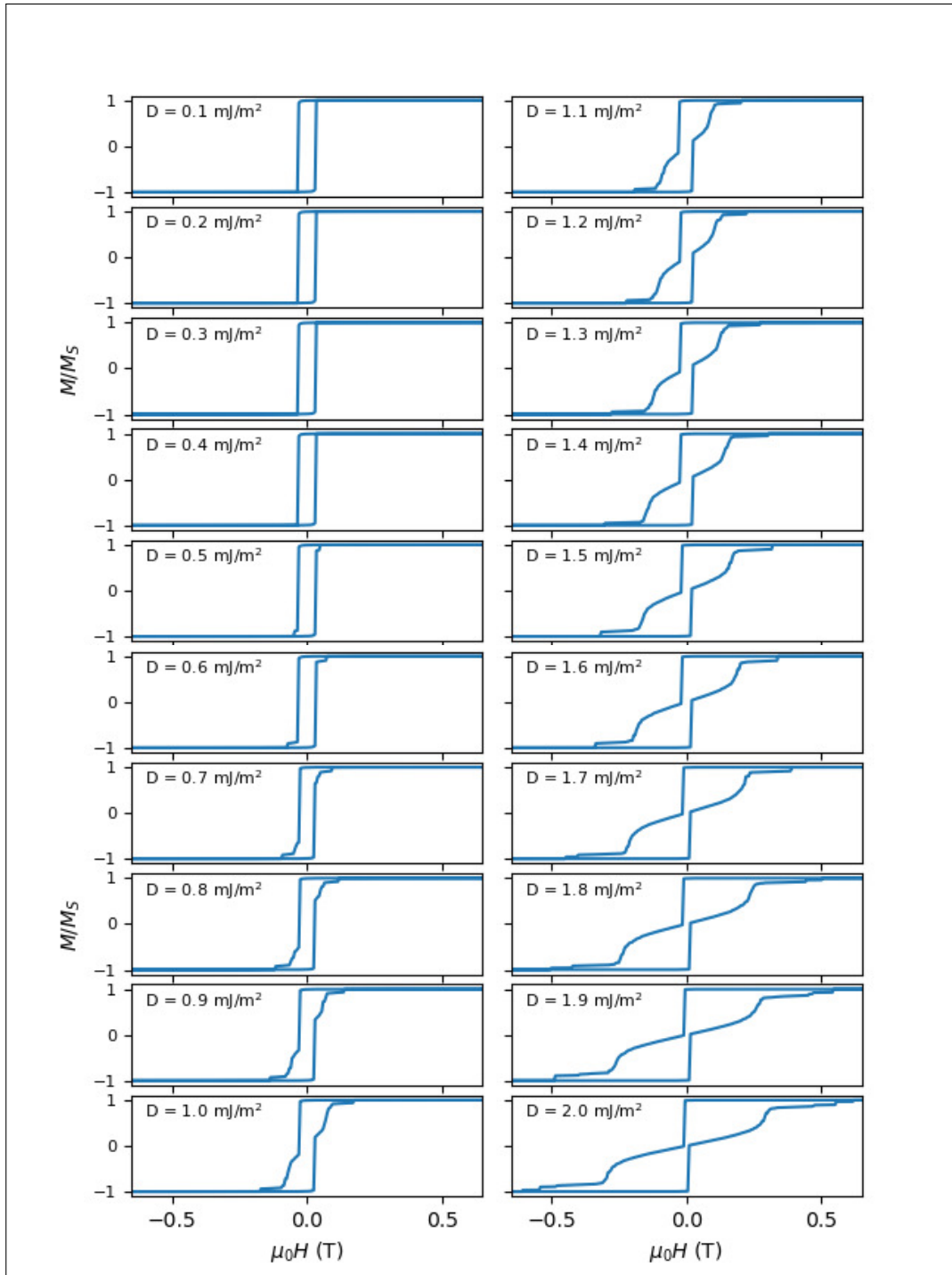
Figure 6 – Hysteresis loops obtained for intermediary anisotropy

Figure 7 – Hysteresis loops obtained for high anisotropy